Multiphase numerical analysis of the vortex formation near the suction of the vertically mounted axial-flow pump with influence of the free water level

Prokop Moravec[1,*], *Lukáš* Zavadil[1], *Jakub* Stareček[1], *Tomáš* Krátký[2], and *Milan* Sedlář[1]

[1]SIGMA Research and Development Institute, Department of the hydraulic research, Jana Sigmunda 313, Lutín, Czech Republic

[2]CENTRE OF HYDRAULIC RESEARCH, Jana Sigmunda 313, Lutín, Czech Republic

Abstract. Presented paper deals with the numerical investigation of a flow in a complete hydraulic system of a pump station. The station uses a recently developed high-efficiency axial-flow pump with the specific speed n_s=680 min^{-1}. The pump is vertically mounted in the suction object with the free water level and equipped with the suction bell and the suction cone with one rib. For the numerical simulations, the lowest possible water level is considered. Such scenario is the most limiting for the pump station design and need to be analysed properly. The unsteady multiphase numerical simulations were focused on the creation of the complex vortical structures at the suction part of the mentioned axial-flow pump. This phenomenon strongly influences the pump performance (hydraulic efficiency, delivery and suction head, etc.) and operation (especially the vibrations and noise) characteristics. The unsteady flows inside the investigated domains are simulated using Ansys Fluent with appropriate solver settings. The Scale Resolving Simulations (SRS) are used to model large vortices and the interaction between stationary and rotating parts.

1 Introduction

This paper deals with the numerical analysis of the fluid flow in a complete hydraulic system of a pump station, including the effects of the free water level. Such hydraulic system usually consists of an intake object, one or more pumps, a discharge object and a piping connecting the pump runner to the outlet domain. The presented research is focused on the turbulent flow in the intake object with one pump (fig. 1). There are several references pursuing this topic, using CFD simulations or laboratory measurements [1, 2, 3 and 4].

To investigate possible vortex creation in the vicinity of the pump runner, the lowest possible water level in the intake object is considered. Such regime is the most critical, as with the low water level there is the highest chance of air entering the pump – resulting in serious problems for the pump operation.

Fig. 1. 3D model of the hydraulic pump system.

* Corresponding author: p.moravec@sigma.cz

2 Vortex creation

A creation of the turbulence (small vortices) is typical for any turbulent flow. The large-scale vortex develops in shear flows, where significant velocity gradients strongly dominate. In the vortices, the pressure decreases its value from the border region of a vortex shape to a vortex core. On the free water level, the fluid surface sinks in the vortex core due to a constant gas pressure, which affects the liquid surface [5].

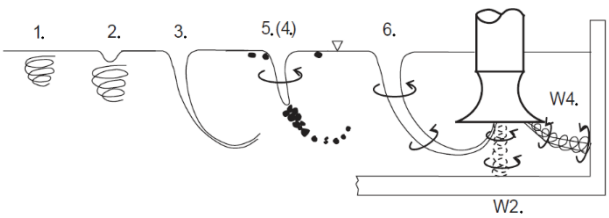

Fig. 2. Types of vortices [5].

When focusing on a vortex strength, several vortex classifications emerge (see fig. 2) [5]:

Free surface vortices [5]:

1. Swirl visible on liquid level.
2. Surface dimple.
3. Dye core to intake.
4. Vortex pulling trash (not air) to intake.
5. Vortex pulling air bubbles to intake.

6. Vortex pulling air continuously to intake.

Submerged vortices [5]:

W1. Weak swirl (no coherent core).
W2. Coherent dye core.
W3. Organized air core (air separation).
W4. Vapour core (strong cavitation noise).

The generation of the vortices has a significant impact on the pump operation and can cause following unfavourable phenomena [5]:

- Power, efficiency, head and flow rate change.
- Vibrations and noise.
- Hydraulic excitation forces increase.

The related energy dissipation means lower efficiency and has adverse effect on the pump performance. Thus, it is crucial to consider the effects of vortices for the hydraulic system design.

3 CFD

All numerical simulations were performed with commercial software ANSYS Fluent (release 2019R3 [6]). The Volume-of-Fluid (VOF) method, combined with the SIMPLE pressure-velocity coupling and PRESTO! pressure interpolating scheme, was used for the numerical solution of the free-surface flow. The simulation was fully-transient, with timestep matching 360 or alternatively 360 steps during one impeller revolution (i.e. one or two degrees of impeller blades movement). SAS model of turbulence was used. To correctly capture the fluid flow inside the investigated domains, gravity effects (acceleration constant g = 9.81 m/s^2) were also considered.

The computational mesh was assembled from four parts - computational domains (intake object, pump impeller, diffuser and the piping). In the computational model, the domains are connected via interfaces. The impeller was set as moving (rotating) domain, the remaining domains were stationary. The mesh size was about 14 million nodes (7 million cells) and combined together hexahedral, tetrahedral and polyhedral elements (fig. 3).

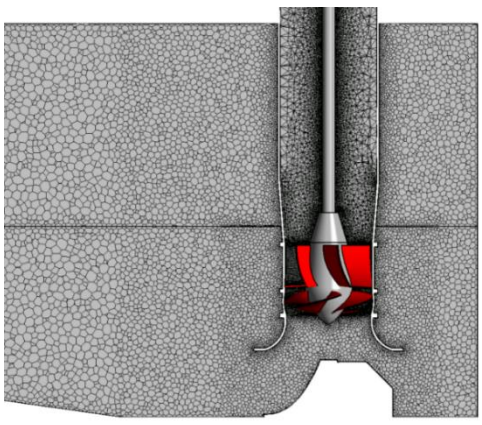

Fig. 3. Computational mesh (blades are shown in red).

3.1. Pre-processing

3.1.1 Intake object and piping

The intake object provided prescribed volume flow rate towards the pump impeller (Q = 4 m^3/s). It consists of a pump chamber with suction bell, a splitter and the free water level, which is located in the distance of 2.3 m from an object intake base wall (fig. 4).

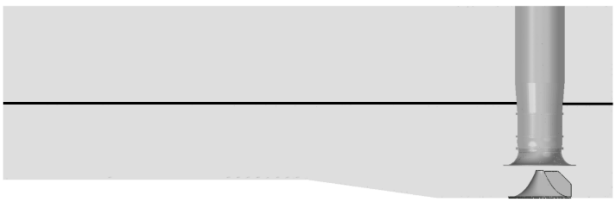

Fig. 4. Water level (the black line) in the intake object.

The connecting piping connects (fig. 5) the pump's outlet and the water tank. As the water has only negligible impact the pump intake, it is neglected in our CFD model, and replaced by an outlet boundary condition (represented by Outflow and located 15*D_{pump} from a pipe elbow). This is helping in keeping reasonable size and complexity of the computational mesh. This domain also contains moving walls of the hub and shaft. Such walls rotate with the same RPM and direction as the pump impeller.

Fig. 5. Connecting piping and shaft.

3.1.2 Pump impeller and distributor

The pump station is based on a recently developed high-efficiency axial-flow pump with specific speed n_s = 680 min^{-1}. It has five impeller and six distributor (diffuser) blades (fig. 6). The outer diameter of the impeller is D_{pump} = 1072 mm and RPM = 380 min^{-1}.

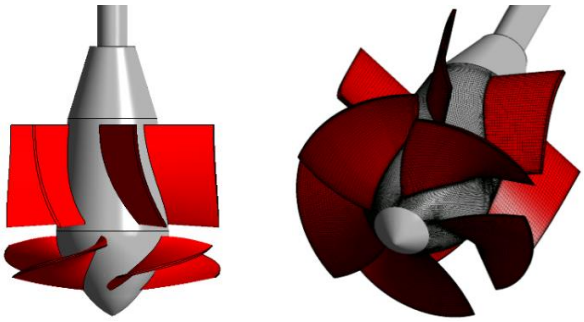

Fig. 6. Pump impeller and distributor (diffuser). Geometry (left) and surface mesh (right).

3.2 Post-processing and results evaluation

For the proper evaluation of the unsteady numerical simulations of the fluid flow inside the investigated pump hydraulic system served CFD-Post, part of the commercial ANSYS software package.

Figures 7-9 show a comparison between data from two separate timesteps of the calculation – first is from the timestep $t_1 = 0.324$ [s], the second one from $t_2 = 0.648$ [s]. A time difference equals to $\Delta t = 0.324$ [s].

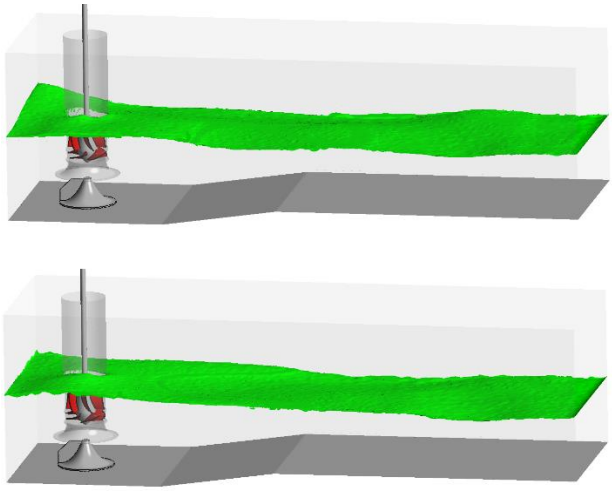

Fig. 7. Free water level – two different values of timestep.

Figure 7 illustratively shows the free water level (portrayed by the green colour) inside the intake object of the investigated hydraulic system. A visualization is done by using of an isosurface of a water fraction ($\alpha_{water} = 0.5$). On the top of the figure 7 is located the first observed timestep $t_1 = 0.324$ [s], on the bottom is $t_2 = 0.648$ [s]. Both cases show mild water level distortion in the close surroundings of the suction part of the pump. Such distortion afterwards propagates itself towards the inlet part of the intake object – a noticeable wave-like instability could be observed.

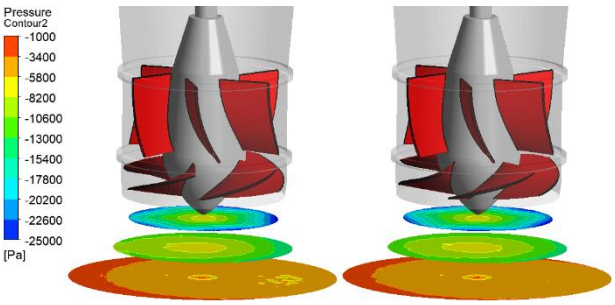

Fig. 8. Static pressure in the suction bell.

Figure 8 compares static pressure distributions inside the suction bell of the pump configuration of the two chosen observed timesteps. The static pressure was evaluated on three horizontal planes, which were equally inserted into the suction part of the pump. Both of these distributions show similar values and qualities, with relatively higher values in front of the pump hub towards the splitter (middle section of each evaluated horizontal plane).

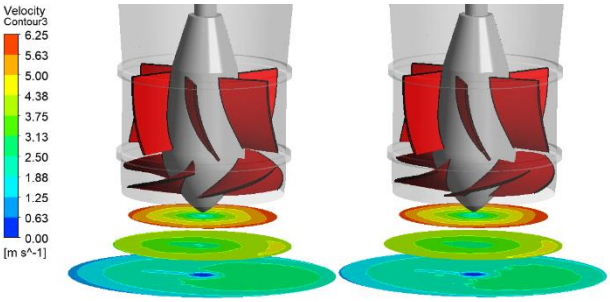

Fig. 9. Velocity in the suction bell.

On the same planes as were defined and displayed in figure 8, values of the velocity in the stationary frame were shown. The rotation of the impeller strongly influences fluid (water) behaviour in the suction part of the pump. The liquid is accelerated by this movement, which is afterwards propagated as a circular change of the velocity (fig. 9).

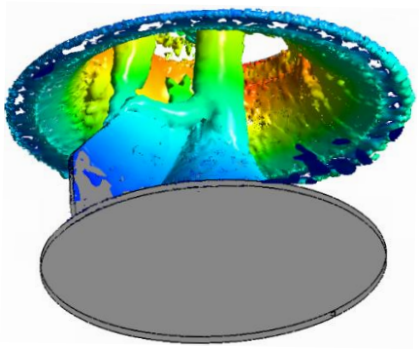

Fig. 10. Vortices in the suction bell of the pump in t_1.

As it was mentioned above, larger vortical structures usually manifest in the flow, where significant velocity gradients dominate. Figures 10-11 show isosurfaces of an absolute helicity coloured by the water velocity inside the suction bell of the pump (warmer colours represent higher velocities, colder colours the other way around). The isosurface in figure 10 uncovers the two main vortical structures: first vortical structure continuously attaches to the tip of the hub, the second structure heads toward the splitter, where it is successfully eliminated by the shape of the splitter.

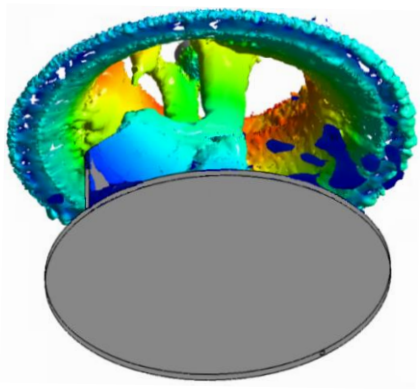

Fig. 11. Vortices in the suction bell of the pump in t_2.

Figure 11 captures vortical structures in the observed timestep t_2. There are three main vortices, which are situated in close surroundings of the tip of the impeller hub. One vortex is undeveloped, the rest heads toward the splitter, and where the vortex grow is limited. No vortical structures from the free water level towards the impeller were detected.

Following six figures show the pressure and velocity distributions in the horizontal plane (XY plane) that passes through a centre of the impeller of the axial-flow pump (z = 1.4 [m]).

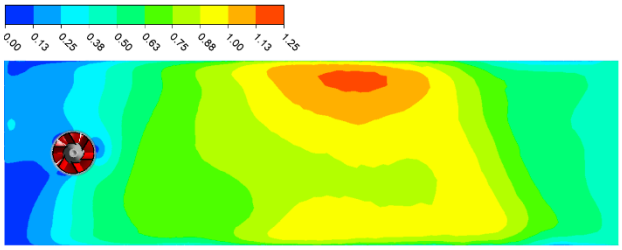

Fig. 12. Contours of the velocity in the stationary frame in t_1.

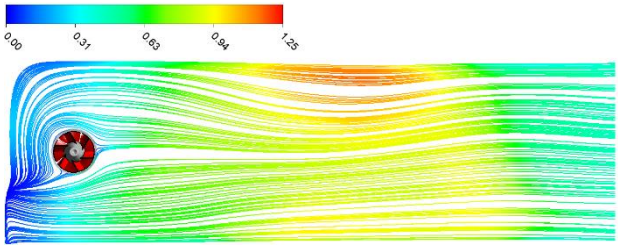

Fig. 13. 2D streamlines coloured by the velocity (timestep t_1).

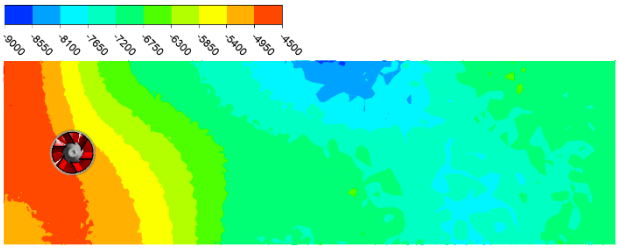

Fig. 14. Contours of the static pressure in t_1.

In the timestep t_1, higher velocity (lower static pressure) values are visible in the middle section of the intake object. This is caused by the deformation of the free water surface, which is in this location slightly lowered. Behind the impeller the water is decelerated due to an interaction with the wall of the intake object.

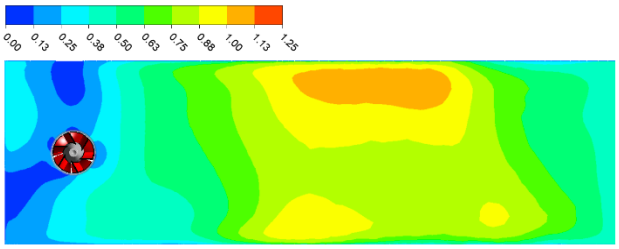

Fig. 15. Contours of the velocity in the stationary frame in t_2.

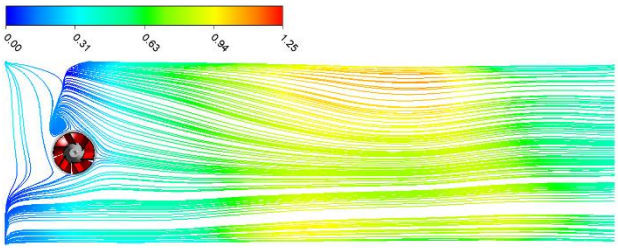

Fig. 16. 2D streamlines coloured by the velocity (timestep t_2).

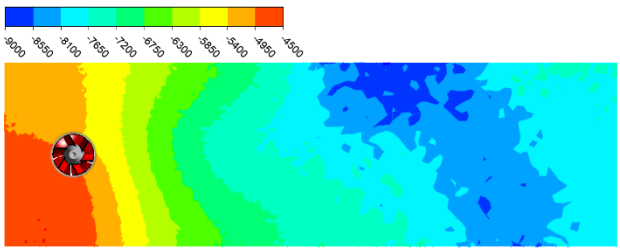

Fig. 17. Contours of the static pressure in t_2.

The timestep t_2 also indicates lowered free water level located in the middle section of the intake object, which is characterized by higher velocity (lower static pressure) values. The major difference between the two selected timesteps can be observed in a visualization of the 2D streamlines (figures 13 and 16). The plane (z = 1.4 [m]) in the timestep t_2 uncovers minor flow instability, which is formed around a part of the impeller chamber. Such instability dissipates energy and can consequently negatively influences fluid entering the suction and lower the pump performance.

4 Conclusion

Presented research was focused on the intake object of the hydraulic pump system, more precisely on the standard operation regime of the axial-flow pump in such system (the optimal volume flow rate). The examined layout was based on the recently developed high-efficiency axial-flow pump with the specific speed n_s = 680 min^{-1} (see figure 6). This pump was mounted in the intake object, where the free water level was set to its minimal possible height. The outlet domain was substituted by the piping system with the elbow. The minimal possible height of the water level is the most critical condition, in which is the highest probability of the creation of the vortical structures towards the free water level that can negatively affect the correct pump behaviour (air pulling towards the impeller, vibrations, noise, impact on the performance characteristics, cavitation).

The numerical simulations of the two-phase fluid flow using the commercial software ANSYS Fluent (release 2019R3) with chosen SAS model of the turbulence were employed. Two different timesteps were selected to demonstrate the water (and consequently air) behaviour during the examined pump run (data from 0.324 and 0.648 [s] of the pump run). The water level representation (green surface in figure 7) shows only the mild type of the deformation in the close vicinity of the impeller (only the wave-like instabilities were observed)

– no major height decrease/lowering on a local scale that could indicate the vortex creation towards the free water level.

The contours of the velocity in the stationary frame near the pump impeller (displayed on the chosen XY plane – figures 12 and 15) uncovered only the significant water deceleration caused by the interaction with the solid walls of the intake object.

The vortical structures were presented only in the suction bell area (in front of the pump impeller). Their behaviour was unsteady – the duration and count varied in time. Those structures tended to connect with the top part of the splitter. Bigger vortical structures (towards the free water level or towards the solid side of the intake object) were successfully eliminated by the splitter, which is located in the bottom of the intake object (see figures 10-11).

It must be noted that the presented numerical simulations captured only a small fraction of the real pump run that usually lasts in hours or days. The flow simulations were also free of the additional solid particles that may initiate the formation of the vortical structures.

This research was funded by the Ministry of Education, Youth and Sports of the Czech Republic, grant number CZ.02.1.01/0.0/0.0/17_049/0008408. Computational resources were supplied by the project "e-Infrastruktura CZ" (e-INFRA CZ LM2018140) supported by the Ministry of Education, Youth and Sports of the Czech Republic.

References

1. T. Okamura, K. Kamemoto, J. Matsui, CFD prediction and model experiment on suction vortices in pump sump, Proc. 9th Asian Int. Conf. on Fluid Machinery (2007) 1-10.
2. S.N. Shukla, J.T. Kshirsagar, Numerical prediction of air entrainment in pump intakes, Proc. 24th Int. Pump Users Symposium (2008) 29-33.
3. A.C. Bayeul-Lainé, G. Bois, A. Issa, Numerical simulation of flow field in water-pump sump and inlet suction pipe, Proc. 25th IAHR Symp. on Hydraulic Machinery and Systems (2010) 1-8.
4. C.G. Kim, B.H. Kim, B.H. Bang, Y.H. Lee, Experimental and CFD analysis for prediction of vortex and swirl angle in the pump sump station model, IOP Conf. Series: Materials Science and Engineering 72 (2015) 042044, doi:10.1088/1757-99X/72/4/0420.
5. J. F. Gülich, Centrifugal pumps, 3rd edition. Heidelberg: Springer, 2014, xli, p. 1116. ISBN 978-3-642-40113-8.
6. ANSYS, Inc., ANSYS CFD Documentation, Release 2019R3 (2019).